

This is the accepted manuscript made available via CHORUS. The article has been published as:

Kinetic Ising models with self-interaction: Sequential and parallel updating

Vahini Reddy Nareddy and Jonathan Machta

Phys. Rev. E **101**, 012122 — Published 15 January 2020

DOI: [10.1103/PhysRevE.101.012122](https://doi.org/10.1103/PhysRevE.101.012122)

Kinetic Ising Models with Self-interaction: Sequential and Parallel Updating

Vahini Reddy Nareddy^{1,*} and Jonathan Machta^{1,2,†}

¹*Department of Physics, University of Massachusetts, Amherst, Massachusetts 01003 USA*

²*Santa Fe Institute, 1399 Hyde Park Road, Santa Fe, New Mexico 87501, USA*

Abstract

Kinetic Ising models on the square lattice with both nearest-neighbor interactions and self-interaction are studied for the cases of random sequential updating and parallel updating. The equilibrium phase diagrams and critical dynamics are studied using Monte Carlo simulations and analytic approximations. The Hamiltonians appearing in the Gibbs distribution describing the equilibrium properties differ for sequential and parallel updating but in both cases feature multispin and non-nearest-neighbor couplings. For parallel updating the system is a probabilistic cellular automaton and the equilibrium distribution satisfies detailed balance with respect to the dynamics [E. N. M. Cirillo, P. Y. Louis, W. M. Ruszel and C. Spitoni, *Chaos, Solitons and Fractals*, 64:36(2014)]. In the limit of weak self-interaction for parallel dynamics, odd and even sublattices are nearly decoupled and checkerboard patterns are present in the critical and low temperature regimes, leading to singular behavior in the shape of the critical line. For sequential updating the equilibrium Gibbs distribution satisfies global balance but not detailed balance and the Hamiltonian is obtained perturbatively in the limit of weak nearest-neighbor dynamical interactions. In the limit of strong self-interaction the equilibrium properties for both parallel and sequential updating are described by a nearest-neighbor Hamiltonian with twice the interaction strength of the dynamical model.

PACS numbers: 75.40.Mg, 05.50.+q, 64.60.-i

* vnareddy@umass.edu

† machta@physics.umass.edu

I. INTRODUCTION

Kinetic Ising models, broadly defined, are systems of Ising spins equipped with a dynamical rule for updating the spin configuration. Kinetic Ising models have been investigated in many settings and play a fundamental role in understanding non-equilibrium processes, in modelling the dynamics of more complex systems and as computational tools for studying equilibrium systems through the use of Markov chain Monte Carlo. The most commonly used kinetic Ising models update spins sequentially and determine the new spin state probabilistically from the current state of the neighboring spins using update rules such as heat bath dynamics or Metropolis dynamics. In this paper we study kinetic Ising models with a self-interaction or memory term so that the new state of the spin also depends on the current state of the spin itself. We consider this kinetic Ising model both with random sequential and parallel updating. The parallel version of the model is an example of a probabilistic cellular automata and many of its properties are understood [1, 2]. The sequential version of the model violates detailed balance when the self-interaction term is finite but non-vanishing and has received less attention.

Dynamical Ising-like systems with self-interaction have also been proposed to model a variety of systems including neural networks [3], financial markets [4] and opinion dynamics [5]. The addition of a memory term has also been proposed as a method to accelerate Monte Carlo simulations [6]. We were motivated to study the kinetic Ising model with memory as a reduced description of synchronous ecological populations described by coupled, noisy oscillators. When each oscillator is individually in a two-cycle regime, the phase of the two-cycle can be represented by an Ising spin. As a function of noise and coupling strength, these systems undergo a phase transition to synchronous oscillation, which can be mapped to an ordering transition in the Ising universality class [7]. However, to model dynamic and non-universal properties of the coupled oscillator system it is necessary to include memory in the Ising representation since each oscillator remembers its own phase for an extended period, even in the absence of coupling to its neighbors.

The paper is organized as follows. In Sec. II, we introduce the sequential and parallel kinetic Ising models with self-interaction and describe our numerical methods. In Sec. III we present numerical results for the equilibrium phase diagram of both models and the dynamic properties along the critical lines. In Sec. IV we analyze the equilibrium states of the parallel and sequential models and derive associated Hamiltonians. In the case of parallel dynamics we focus on the weak self-interaction regime where the critical line displays singular behavior. For the sequential case, we derive the equilibrium Hamiltonian from the global balance equations in a weak coupling expansion. We also study the nontrivial case of parallel updating in standard Ising model with no memory. In Sec. V we develop a mean field approximation to the kinetic Ising model with self-interaction. The paper concludes with a discussion.

II. MODEL AND NUMERICAL METHODS

We consider kinetic Ising models with both nearest-neighbor interactions and self-interaction or, equivalently, memory. The system consists of N Ising spins, $S_i = \pm 1$ and $i = 1, 2, \dots, N$, on a two-dimensional square lattice of even size with periodic boundary conditions. The dynamics of the system is defined by the transition probability, $A(\alpha \rightarrow \gamma)$ between successive configurations of the system α and γ . We consider two types of heat bath dynamics, parallel and sequential. In both cases the transition probabilities are controlled by the single-spin marginal probability $p(S_i^\gamma|\alpha)$ for finding spin at site i in the new configuration γ , S_i^γ , given the initial configuration α ,

$$p(S_i^\gamma|\alpha) = \frac{\exp[(Jh_i^\alpha + KS_i^\alpha)S_i^\gamma]}{2 \cosh(Jh_i^\alpha + KS_i^\alpha)}. \quad (1)$$

Here J is the dimensionless nearest-neighbor interaction and K is the dimensionless self-interaction. The local field, h_i^α is the sum over spins S_j^α where j is a neighboring site of i ,

$$h_i^\alpha = \sum_{\langle j;i \rangle} S_j^\alpha. \quad (2)$$

The notation $\langle j;i \rangle$ indicates that the summation variable j is a nearest neighbor of i . In what follows we omit the superscripts specifying the configuration where no confusion results.

Sequential dynamics For random sequential dynamics the transition probability $A_s(\alpha \rightarrow \gamma)$ for $\gamma \neq \alpha$ is given by,

$$A_s(\alpha \rightarrow \gamma) = \frac{1}{N} \sum_i \chi_1(\alpha, \gamma, i) p(S_i^\gamma|\alpha), \quad (3)$$

where $\chi_1(\alpha, \gamma, i)$ is an indicator function that forces α and γ to differ only on S_i , that is $\chi_1(\alpha, \gamma, i) = 1$ if $S_i^\gamma = -S_i^\alpha$ and $S_j^\gamma = S_j^\alpha$ for all $j \neq i$, while $\chi_1(\alpha, \gamma, i) = 0$ otherwise. The probability for no transition, $A_s(\alpha \rightarrow \alpha)$ is obtained, as usual, from normalization. For $K = 0$, sequential dynamics is standard heat bath dynamics.

In simulations, a single step of the sequential dynamics consists of choosing a site i at random and then choosing the spin state S_i according to the probability $p(S_i|\alpha)$. The result is the new state γ .

Parallel dynamics For parallel dynamics all spins are updated at the same time and the transition probability $A_p(\alpha \rightarrow \gamma)$ is given by

$$A_p(\alpha \rightarrow \gamma) = \prod_i p(S_i^\gamma|\alpha). \quad (4)$$

For $K = 0$, parallel dynamics on a bipartite graph permits period-two oscillatory states. For example, if J is sufficiently large, the system may oscillate between the two “checkerboard” states (i.e. ground states of the Ising antiferromagnet). The Ising model with parallel dynamics is an example of a probabilistic cellular automaton [2, 8, 9].

We carried out extensive simulations of both parallel and sequential dynamics with the primary goal of understanding the static and dynamic critical properties of the models. To identify the critical points of the models for various values of K we used the Binder cumulant method. The fourth-order Binder cumulant for the magnetization is given by [10],

$$U = 1 - \frac{\langle M^4 \rangle}{3\langle M^2 \rangle^2}, \quad (5)$$

where $M = \frac{1}{N} \sum_i S_i$ is the magnetization per spin. At low temperatures, in the ferromagnetic phase, the Binder cumulant takes the value $2/3$ whereas it goes to zero in paramagnetic phase. At the phase transition, the critical Binder cumulant for the standard Ising model on the 2D square lattice with periodic boundary conditions is $U^* \approx 0.61069$ [11]. The value of the critical coupling is obtained from crossing of the Binder cumulant curves for different system sizes. For parallel dynamics and small values of K we also make use of a sublattice Binder cumulant to find critical points for reasons discussed in Sec. IV A 1.

The dynamics of the sequential model are studied using the magnetization integrated autocorrelation time defined from the magnetization autocorrelation function,

$$\Gamma_M(t) = \frac{\langle M(t)M(0) \rangle - \langle M \rangle^2}{\langle M^2 \rangle - \langle M \rangle^2}.$$

Here time is measured in Monte Carlo sweeps and the integrated autocorrelation time, τ is defined as,

$$\tau = \frac{1}{2} + \sum_{t=1}^{\infty} \Gamma_M(t). \quad (6)$$

Care must be taken in estimating τ from numerical data for $\Gamma_M(t)$ since an upper cut-off is required on the sum. If the cut-off is too small the estimate will have large systematic errors and if it is too large it will have large statistical errors. We follow the procedure described in Ref. [12] for choosing the cut-off.

We have carried out simulations of both the parallel and sequential models for multiple values of $K > 0$ for lattice sizes varying from $L = 10$ to 120. The critical dynamic couplings, $J_c^{(p)}(K)$ and $J_c^{(s)}(K)$, for the parallel and sequential cases, respectively, are estimated from the crossing points of the Binder cumulant curves for two lattice sizes. The crossing point were found for sizes $L = 30$ and 60, except for the data presented in Sec. IV A 1, where two sizes were $L = 100$ and 120. Each Binder cumulant data point is averaged over 40 independent runs for the sequential results and 20 independent runs for parallel results. Each run consists of S Monte Carlo sweeps including an initial S_b sweeps for equilibration. Observables are averaged over the remaining $S - S_b$ sweeps. For the sequential model, $S = 7 \times 10^7$ and $S_b = 5 \times 10^7$ while, for the parallel model, $S = 4 \times 10^7$ and $S_b = 2 \times 10^7$ except for the data presented in Sec. IV A 1 where $S = 8 \times 10^7$ and $S_b = 5 \times 10^7$.

III. STATIC AND DYNAMIC CRITICAL BEHAVIOR

A. Phase diagrams

The phase diagrams for sequential and parallel dynamics are plotted in Fig. 1. Critical values of the dynamic couplings, $J_c^{(s)}(K)$ and $J_c^{(p)}(K)$, for sequential and parallel dynamics, respectively, and for various values of K are obtained from crossings of the Binder cumulant as discussed above. The ferromagnetic phase lies above the points and the paramagnetic phase below the points. As expected, as $K \rightarrow 0$, the critical lines both approach $J_c(0) \approx 0.4407$, the critical value of the standard nearest-neighbor square-lattice Ising model. Furthermore, as discussed in Sec. IV, for K large, both lines approach $J_c(0)/2$. The numerical result $J_c^{(p)}(K = 0.31) \approx 0.31$ agrees well with the value $J_c^{(p)}(K = 0.31) \approx 0.32$ obtained from Monte Carlo simulations in Ref. [9].

The solid curves in Fig. 1 are approximations to the critical lines for the two dynamics. For parallel dynamics, the approximation is a fit with two hyperbolic tangent functions that represent crossovers from power-law behavior expected for small K and the asymptotic values $J_c(0)/2$ for large K . The fit takes the form,

$$J_c^{(p)}(K) = J_c(0) \left[1 - \frac{1}{2} \tanh(aK) \right] - dK^c [1 - \tanh(bK)], \quad (7)$$

with the best fit parameters $a = 1.17$, $b = 1.46$, $c = 0.45$, and $d = 0.15$. A more detailed analysis of the power-law behavior in K is presented in Sec. IV A 1.

The solid curve in Fig. 1 for sequential dynamics is obtained from an approximation to the Hamiltonian for sequential dynamics that is obtained in Sec. IV B 1 and is defined in Eq. (64).

We have not investigated the static critical properties along the critical lines however we find that the Binder cumulant takes the universal Ising value (except near $K = 0$ for the parallel case, as discussed in Sec. IV A 1), supporting general arguments [1] that kinetic models with self-interaction are in the Ising universality class.

B. Autocorrelation time for sequential dynamics

Along the critical line, τ is expected to behave asymptotically in lattice size, L as a power law,

$$\tau(K, L) \sim A(K) L^{z(K)} \quad (8)$$

where the amplitude A and dynamic exponent z could, in principle, both be functions of K .

We obtained values of τ for lattice sizes from $L = 10$ to 100 and for different values of K . The results for τ as a function of L for $K = 1.23$ are shown in Fig. 2. The solid line is a fit to $\tau = AL^z$ with fitted values $z = 2.15$ and $A = 0.16$ ($\chi^2/\text{d.o.f} = 1.38$).

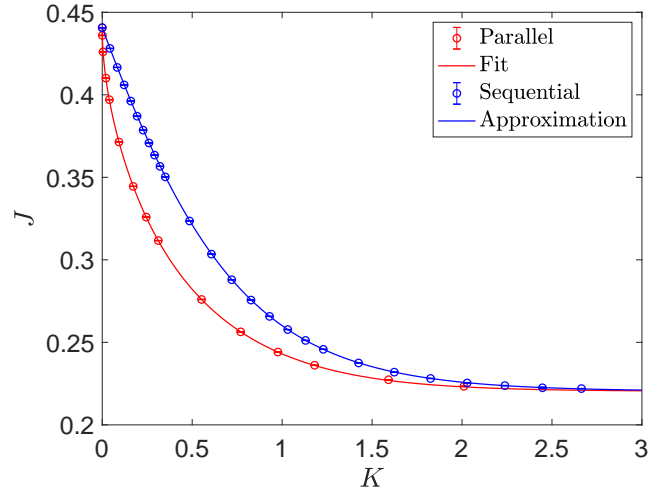


Figure 1. The phase diagram in the J - K plane shows the critical dynamical couplings, $J_c^{(s)}(K)$ and $J_c^{(p)}(K)$, for sequential (blue points, upper) and parallel (red points, lower) dynamics, respectively. The red solid line represents a fit for the critical line for parallel dynamics (see Eq. (7)). The blue solid line represents an approximation to the sequential critical line that is described in Sec. IV B 1.

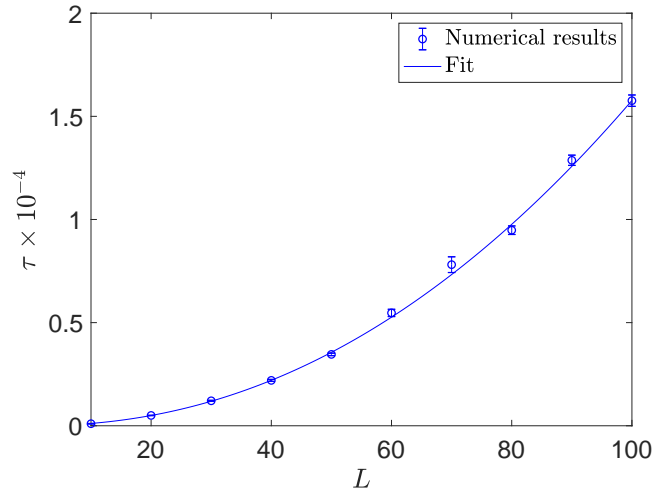


Figure 2. The magnetization integrated autocorrelation time for sequential dynamics, τ as a function of lattice size L for $K = 1.23$. The solid line is a fit to $\tau = AL^z$ with fitted values $A = 0.16$ and $z = 2.15$.

Figure 3 shows $z(K)$ as a function of K obtained from fits of the form $\tau = AL^z$. The values of $z(K)$ are all reasonably close to the accepted dynamic exponent of the 2D Ising model with non-conserved order parameter, $z = 2.16$ [13–15], with no discernable trends in K . We believe that the kinetic Ising model with self-interaction is in the dynamic Ising universality class with a non-conserved order parameter (Model A of [16]) and that the deviations in the measurements from $z(K) = z(0)$ result from a combination of finite-size corrections and statistical errors. This conclusion is in agreement with the result that systems with local dynamics and a non-conserved order parameter are in universality class of Ising models [1, 17].

We now assume z takes the universal value, 2.16 and investigate the prefactor, $A(K)$. The autocorre-

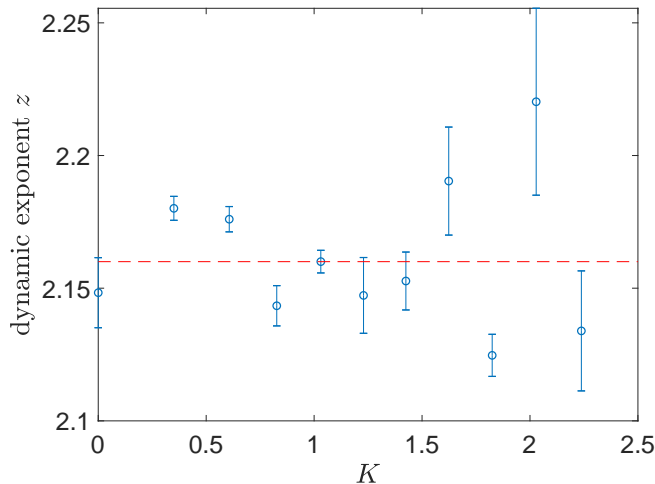


Figure 3. Dynamic exponent z for the autocorrelation time (see Eq. (8)) is obtained as a function of self-interaction K for sequential dynamics. The dashed horizontal line denotes the non-conserved order parameter Ising universal dynamic exponent, $z = 2.16$.

lation time τ is fitted to the form,

$$\tau(K, L) = A(K)L^{2.16} + B(K), \quad (9)$$

where the constant $B(K)$ is included to improve the quality of the fit. The numerical results for the amplitude function $A(K)$ are obtained for various values of K and are shown for sequential updating in Fig. 4. The data can be fit to the form,

$$A(K) = a[1 + b \exp(2K)], \quad (10)$$

with the best fit parameters, $a = 0.09$ and $b = 0.64$ ($\chi^2/\text{d.o.f} = 0.99$). The fit is shown as a solid line in the figure. The factor $\exp(2K)$ is the time scale between spin flips for an isolated spin with self-interaction and this time scale apparently controls the asymptotic behavior of $A(K)$. Although the above results are for sequential dynamics, in the limit of large K , when the time scale for spin flips is much larger than the number of spins, parallel and sequential dynamics are expected to have the same dynamical properties.

IV. EQUILIBRIUM STATES

The kinetic Ising models with self-interaction ultimately reach an equilibrium state, which can be written in the form of a Gibbs distribution with a dimensionless Hamiltonian, \mathcal{H} so that the probability of a configuration α is given by $P(\alpha) = \exp[-\mathcal{H}(\alpha)]/Z$ with Z the partition function. This probability and its associated Hamiltonian must satisfy global balance with respect to the transition probabilities,

$$\sum_{\gamma} [P(\gamma)A(\gamma \rightarrow \alpha) - P(\alpha)A(\alpha \rightarrow \gamma)] = 0, \quad (11)$$

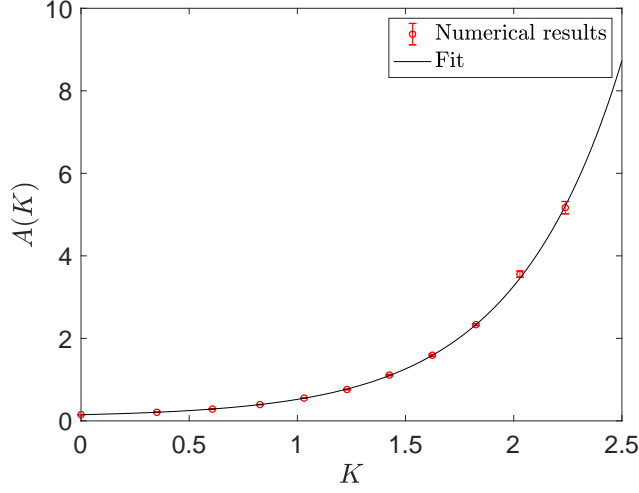


Figure 4. The amplitude $A(K)$ of the autocorrelation time divergence at criticality (see Eq. (9)) is plotted as a function of K for sequential updating. The solid line is the fit $A(K) = 0.09[1 + 0.64 \exp(2K)]$.

for all α . For the case of parallel dynamics, the Hamiltonian satisfies detailed balance and was obtained in Ref. [2]. The derivation and resulting Hamiltonian is presented in Sec. IV A. The Hamiltonian for the sequential case is discussed in Sec. IV B. It does not satisfy detailed balance and we have only been able to obtain it as an expansion in powers of J . For both parallel and sequential cases, the Hamiltonians contain more than nearest-neighbor, two-spin interactions.

A. Parallel dynamics

From Eqs. (1) and (4), the transition probability for parallel dynamics can be written as,

$$A(\alpha \rightarrow \gamma) = \prod_i \frac{\exp(Jh_i^\alpha S_i^\gamma + K S_i^\alpha S_i^\gamma)}{2 \cosh(Jh_i^\alpha + K S_i^\alpha)}, \quad (12)$$

so that to satisfy detailed balance we required that,

$$\frac{P(\gamma)}{P(\alpha)} = \prod_i \frac{\cosh(Jh_i^\gamma + K S_i^\gamma)}{\cosh(Jh_i^\alpha + K S_i^\alpha)}, \quad (13)$$

and the Hamiltonian \mathcal{H} can be written as [8],

$$-\mathcal{H} = \sum_i \log[\cosh(Jh_i + K S_i)]. \quad (14)$$

From Eq. (13), we should note that in the limit of $K \rightarrow \infty$,

$$\frac{P(\gamma)}{P(\alpha)} = \prod_i \frac{\cosh(Jh_i^\gamma S_i^\gamma + K)}{\cosh(Jh_i^\alpha S_i^\alpha + K)} \rightarrow \prod_i \frac{\exp(Jh_i^\gamma S_i^\gamma)}{\exp(Jh_i^\alpha S_i^\alpha)},$$

which implies that,

$$-\mathcal{H} \rightarrow J \sum_i h_i S_i = 2J \sum_{\langle i,j \rangle} S_i S_j, \quad (15)$$

where the notation $\sum_{\langle 1 \rangle}$ indicates a sum over all nearest-neighbor pairs. Thus, in this limit the Hamiltonian reduces to the standard Ising model with interaction strength twice that of the original kinetic model. This fact has been proved in Ref. [18]. In case of $K \rightarrow -\infty$ we have that,

$$-\mathcal{H} \rightarrow -J \sum_i h_i S_i = -2J \sum_{\langle i,j \rangle 1} S_i S_j, \quad (16)$$

showing that the system behaves as an antiferromagnetic Ising model, again with twice the strength of the interaction in the original dynamical model.

The expression for the Hamiltonian, Eq. (14), can be expanded as a sum of all products of each spin and its four nearest neighbors with various couplings,

$$-\mathcal{H} = J_1 \sum_{\langle i,j \rangle 1} S_i S_j + J_2 \sum_{\langle i,j \rangle 2} S_i S_j + J_3 \sum_{\langle i,j \rangle 3} S_i S_j + T_4 \sum_{\langle i,j,k,l \rangle \perp} S_i S_j S_k S_l + F_4 \sum_{\langle i,j,k,l \rangle \diamond} S_i S_j S_k S_l + C \quad (17)$$

The definitions of the three two-spin couplings and two four-spin coupling allowed by symmetry are illustrated in the Fig. 5. The sum $\sum_{\langle 1 \rangle}$ is over all pairs of nearest-neighbor spins, whereas $\sum_{\langle 2 \rangle}$ and $\sum_{\langle 3 \rangle}$ are sums over second- and third- nearest-neighbor spins with coupling constants J_2 and J_3 , respectively. $\sum_{\langle \perp \rangle}$ and $\sum_{\langle \diamond \rangle}$ are sums over four spins as shown in Fig. 5. The expressions for the dimensionless couplings $\{J_1, J_2, J_3, T_4, F_4\}$ can be obtained as functions of the dynamical interactions J and K by comparing Eqs. (14) and (17) and are given below [2]:

$$J_1 = \frac{1}{4} \log \frac{\cosh(2J + K)}{\cosh(2J - K)} + \frac{1}{8} \log \frac{\cosh(4J + K)}{\cosh(4J - K)}, \quad (18)$$

$$T_4 = \frac{1}{16} \log \frac{\cosh(4J + K)}{\cosh(4J - K)} - \frac{1}{8} \log \frac{\cosh(2J + K)}{\cosh(2J - K)}, \quad (19)$$

$$J_2 = \frac{1}{8} \log[\cosh(4J + K) \cosh(4J - K)] - \frac{1}{4} \log \cosh(K), \quad (20)$$

$$J_3 = \frac{1}{16} \log[\cosh(4J + K) \cosh(4J - K)] - \frac{1}{8} \log \cosh(K), \quad (21)$$

$$F_4 = \frac{3}{8} \log \cosh(K) - \frac{1}{4} \log[\cosh(2J + K) \cosh(2J - K)] + \frac{1}{16} \log[\cosh(4J + K) \cosh(4J - K)]. \quad (22)$$

The couplings are plotted for $J = 1$ as a function of K in Fig. 6. The couplings $\{J_2, J_3, F_4\}$ given in Eqs. (20)-(22) are even in K whereas the couplings $\{J_1, T_4\}$ given in Eqs. (18) and (19) are odd revealing antiferromagnetic behavior for negative values of K .

The couplings are non-trivial even when the self-interaction is zero and are discussed in the Sec. IV A 1. As K increases, the first nearest neighbor coupling J_1 increases to twice the value of J whereas the other couplings decrease to zero.

1. Weak self-interaction regime

When the self-interaction is zero ($K = 0$), the couplings J_1 and T_4 given in Eqs. (18) and (19) are zero. The non-zero couplings J_2, J_3 and F_4 given in Eqs. (20)-(22) produce interactions only within a single

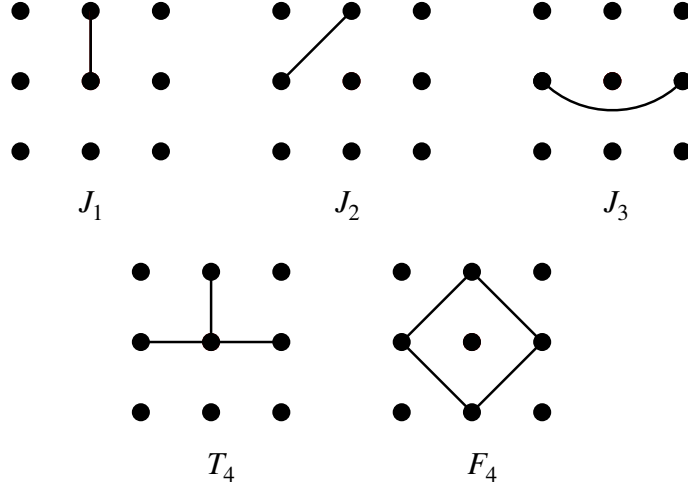


Figure 5. The two-spin couplings, J_1 , J_2 and J_3 couple nearest-neighbor, second-nearest-neighbor and third-nearest-neighbor spins, respectively. The four-spin coupling, T_4 couples a spin with three of its four neighboring spins. The four-spin coupling, F_4 couples the four neighbors of a central spin. All interactions include all rotations and translations of the pictured couplings.

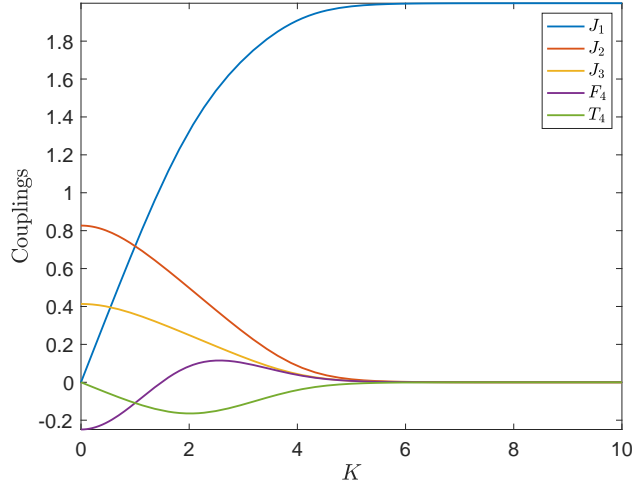


Figure 6. The couplings for parallel dynamics are plotted for $J = 1$ as a function of self-interaction, K as given in Eqs. (18)–(22). For large K , $J_1 \rightarrow 2J$ while the other couplings vanish. Note that J_1 and T_4 are odd functions of K while the other couplings are even.

sublattice. Hence, for $K = 0$ the entire system can be viewed as two independent systems, each on one of the sublattices and with two-spin and four-spin couplings [2, 9].

It is interesting to note that the values of these two- and four-spin couplings given in Eqs. (20)–(22) at $K = 0$ are identical to the expressions for the couplings generated when the real space renormalization group decimation scheme [19, 20] is applied once to the nearest-neighbor Ising model with nearest-neighbor interaction strength J . This observation explains why the parallel update Ising model with $K = 0$ has a critical point at $J_c^{(p)}(0) = J_c(0)$, the critical point of the standard Ising model. A rigorous proof of this fact is given in [9].

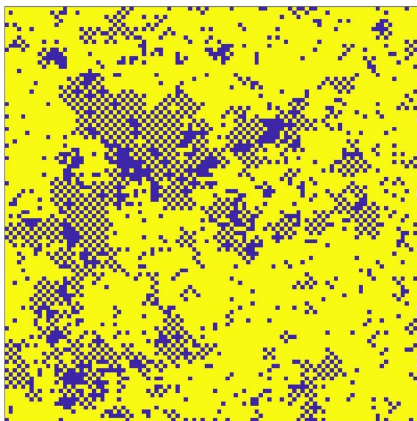


Figure 7. Snapshot of a 100×100 lattice in equilibrium with parallel updating for $K = 4 \times 10^{-4}$ at the critical coupling $J_c^{(p)}(K) = 0.4360$. The presence of large antiferromagnetic clusters result from weak nearest-neighbor interactions (set by J_1) and strong next-nearest-neighbor interactions (set by J_2).

The behavior of the parallel update model for $K = 0$ differs from the standard Ising model because of the presence of two “checkerboard” ground states and, at finite but low temperature, both ferromagnetic and checkerboard ordered phases. The two checkerboard phases each display period-two oscillations between the two antiferromagnetically ordered states and differ in the phase of this oscillation. Furthermore, the four ordered phases each have fluctuations of all four kinds. For example, the ferromagnetic phases will contain checkerboard domains.

As the value of K increases, the couplings that are responsible for interactions between sublattices, J_1 and T_4 , increase. Hence, the sublattices are positively correlated and only the two ferromagnetic ground states survive [2, 8]. However, at finite temperature and K small, checkerboard domains remain common. Figure 7 shows a snapshot of the equilibrium state for $K = 4 \times 10^{-4}$ at the critical coupling, which displays large checkerboard domains. Similarly, for K small and negative, and J near its critical value one finds large ferromagnetic domains.

As can be seen in Fig. 1 and the associated fit, Eq. (7), the critical curve, $J_c^{(p)}(K)$ appears to approach the $K = 0$ critical point, $(J_c(0), 0)$ with infinite slope. The phase diagram is even in K so there is a corresponding critical curve approaching $(J_c(0), 0)$ from negative K . We now give a heuristic argument based on finite-size scaling considerations for the singular behavior of these critical curves near $(J_c(0), 0)$. Near the critical point $(J_c(0), 0)$ there are large fluctuations in both the ordinary (ferromagnetic) magnetization and the staggered (antiferromagnetic) magnetization. These fluctuations are quantified, respectively, by the ordinary susceptibility, χ , and the staggered susceptibility, χ_s , both of which diverge at $(J_c(0), 0)$. Along the critical curve, $J_c^{(p)}(K)$ for $K > 0$, the ordinary susceptibility diverges while along the corresponding critical curve for negative K the staggered susceptibility diverges.

Consider a geometric mean susceptibility, χ_m defined as $\chi_m = \sqrt{\chi\chi_s}$. This mean susceptibility for systems of size L with periodic boundary conditions and with L even is expected to diverge as $L^{\gamma/\nu}$

at $(J_c(0), 0)$. For $K \neq 0$ along the two critical curves, χ_m is expected to have a weaker finite-size divergence, $L^{\gamma/2\nu}$. We now hypothesize that the finite-size scaling behavior of χ_m as a function of L , J and K takes the form,

$$\chi_m(J, K) \approx L^{\gamma/\nu} f((J - J_c(0))L^a, KL^b). \quad (23)$$

The qualitative behavior of the finite-size scaling function $f(x, y)$ is that it has a maximum along the line $y = K = 0$ near $x = 0$. Furthermore, f will decrease in all directions away from the maximum but with two ridge lines near the two critical curves. These ridge lines are expected to take the form $x \sim -(\pm y)^c$ near maximum for the $\pm K > 0$ critical curves, respectively. Given this picture, we must have,

$$(J_c^{(p)}(K) - J_c(0))L^a \sim -(|K|L^b)^c, \quad (24)$$

so that $c = a/b$.

What are the scaling exponents a and b ? Since near $J_c(0)$, J controls the strength of the relevant interactions linearly along the $K = 0$ line, it is reasonable to assume the usual finite-size scaling exponent, $a = 1/\nu$, so, in the present case, $a = 1$.

The exponent b determines the rate of decrease of f for a fixed K as L increases. We hypothesize that this decrease is dominated by the suppression of the “wrong” kinds of fluctuations. For $K > 0$ these are staggered magnetization fluctuations and for $K < 0$ ordinary magnetization fluctuations. For small K the coupling J_1 between sublattices increases linearly in K , specifically (see Eq. (18)), $J_1 = 2JK + O(K^3)$. Thus the energetic cost of the wrong kind of fluctuation of length scale ℓ is given by $2JK\ell^2$ and the wrong kind of fluctuation is suppressed when this energy exceeds $k_B T_c$. The maximum size of these fluctuations is, therefore, $\sqrt{k_B T_c / 2K}$ and the associated finite-size scaling exponent for K is $b = 2$. This estimate ignores the presence of ferromagnetic fluctuations embedded in larger checkerboard regions so that b is expected to be somewhat less than two.

The conclusion of these arguments is that the critical lines approach the $K = 0$ critical point with a singularity,

$$J_c^{(p)}(K) - J_c(0) \sim -|K|^c, \quad (25)$$

and that $c \gtrsim 1/2$.

We obtain numerical results for the critical line for small K using the Binder cumulant method. Care must be taken in using Binder cumulants for small K because the sublattices are nearly uncoupled. Indeed, for $K = 0$ we now show that the Binder cumulant is half its usual value. Let M_1, M_2 be the magnetization of the even and odd sublattices, respectively. The sublattice Binder cumulant is defined by,

$$U_s = 1 - \frac{\langle M_1^4 \rangle}{3\langle M_1^2 \rangle^2}. \quad (26)$$

At the $(J_c(0), 0)$ critical point each sublattice behaves as an independent critical Ising model so U_s will take the Ising critical value for a square lattice with periodic boundary conditions, $U^* \approx 0.61$ [11]. The

full lattice magnetization, M is given by the sum of the two sublattice magnetizations, $M = M_1 + M_2$. Expanding the moments of the full magnetization in terms of the sublattice magnetizations yields,

$$\langle M^2 \rangle = \langle M_1^2 \rangle + \langle M_2^2 \rangle + \langle 2M_1M_2 \rangle \quad (27)$$

$$\langle M^4 \rangle = \langle M_1^4 \rangle + \langle M_2^4 \rangle + \langle 4M_1^3M_2 \rangle + \langle 4M_2^3M_1 \rangle + \langle 6M_1^2M_2^2 \rangle. \quad (28)$$

Since M_1, M_2 are identically distributed, independent random variables we have,

$$\langle M^2 \rangle = 2\langle M_1^2 \rangle \quad (29)$$

$$\langle M^4 \rangle = 2\langle M_1^4 \rangle + 6\langle M_1^2 \rangle^2. \quad (30)$$

Hence, using the definition of the full lattice Binder cumulant, Eq. (5), we have,

$$U = \frac{1}{2} - \frac{\langle M_1^4 \rangle}{6\langle M_1^2 \rangle^2} = \frac{1}{2}U_s. \quad (31)$$

We see that the Binder cumulant of the full lattice for the parallel dynamics, U is half the sublattice Binder cumulant U_s and thus, at criticality it is $(1/2)U^*$. On the other hand, for any $K > 0$ and for sufficiently large L we expect the full lattice Binder cumulant to take the usual Ising value, U^* . Thus, large finite-size corrections are expected for both the full lattice Binder cumulant and also the sublattice Binder cumulants when K is small. The reason for these corrections is the weak coupling between sublattices and the associated presence of large checkerboard domains. We previously estimated that the maximum domain size scales as $\sqrt{J_c(0)/2K}$. For example, if $K = 4 \times 10^{-4}$ this size is about 20, which is comparable to our system sizes.

We have investigated the singular behavior of the critical curve through numerical simulation of five values of K less than 0.1. Here we determine the critical couplings from both the sublattice Binder cumulant and the full lattice Binder cumulant. We use a pair of large system sizes, $L = 100$ and 120 , ($L = 30$ and 60 are used elsewhere) to obtain the crossing of the Binder cumulant curves. The reported values of $J_c^{(p)}(K)$ are obtained by averaging the full lattice and sublattice results in the hope that this procedure will reduce finite-size corrections. Figure 8 shows the numerical results for the critical dynamic coupling ($J_c(0) - J_c^{(p)}(K)$) as a function of K . The error bars shown in the figure are either the difference of the sublattice and full lattice values or the maximum of the statistical errors, whichever is larger. The larger error bars for the three smallest K data points are the result of the large difference between results from the two Binder cumulants and reflect an estimate of the size of systematic errors.

A fit of the data to the form,

$$J_c(0) - J_c^{(p)}(K) = dK^c, \quad (32)$$

yields $c = 0.555 \pm 0.001$ and $d = 0.26$ and ($\chi^2/\text{d.o.f} = 0.83$). This fit is shown as the solid line in Fig. 8. The numerical result for c is consistent with the theoretical arguments presented above. We note that the small error bar on c may be misleading because it is set by the data points with small

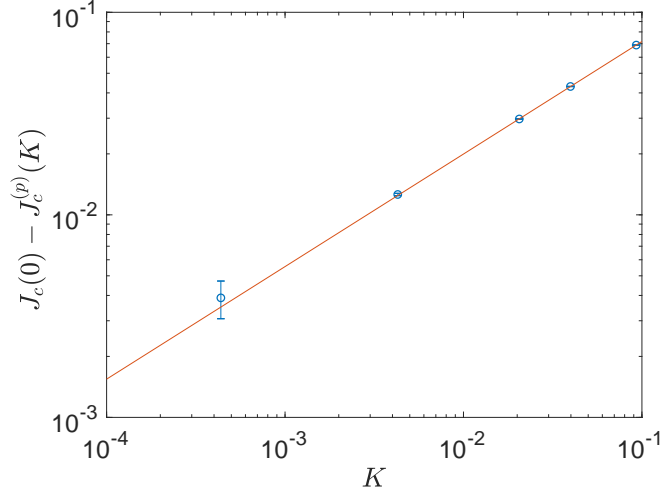


Figure 8. Numerical results for the deviation of the critical dynamic coupling from the Ising critical value, $J_c(0) - J_c^{(p)}(K)$ as a function of K for parallel updating. The solid line is a fit to a power law, by Eq. (32), with exponent $c = 0.555$.

error bars but relatively large values of K , which may hide corrections to scaling in the simple fit, Eq. (32). Independent fits of the sublattice and full lattice results using their respective statistical errors also yield $c \approx 0.55$ but the quality of these fits is poor. It would be interesting to carry out a thorough study of the exponent c and, more generally, the finite-size scaling behavior near the $K = 0$ critical point.

B. Sequential dynamics

From Eqs. (1) and (3), the transition probability when α and γ differ by a single spin flip at site i ($\chi_1(\alpha, \gamma, i) = 1$) is given by,

$$A(\alpha \rightarrow \gamma) = \frac{\exp(Jh_i^\alpha S_i^\gamma + KS_i^\alpha S_i^\gamma)}{2N \cosh(Jh_i^\alpha + KS_i^\alpha)}. \quad (33)$$

First consider the three limiting cases, $K = 0$ and $K \rightarrow \pm\infty$ (holding J fixed), for which detailed balance holds. Note that for sequential dynamics, the neighborhood of S_i is the same for states α and γ so $h_i^\alpha = h_i^\gamma \equiv h_i$. The detailed balance condition is,

$$\frac{P(\gamma)}{P(\alpha)} = \frac{\exp(Jh_i S_i^\gamma)}{\cosh(Jh_i + KS_i^\alpha)} \frac{\cosh(Jh_i + KS_i^\gamma)}{\exp(Jh_i S_i^\alpha)}. \quad (34)$$

For $K = 0$ we have standard heat-bath dynamics,

$$\frac{P(\gamma)}{P(\alpha)} = \exp[Jh_i(S_i^\gamma - S_i^\alpha)], \quad (35)$$

and the equilibrium distribution is that of the standard nearest-neighbor Ising model, $P(\alpha) \propto \exp[(J/2) \sum_i h_i S_i]$. In the limit $K \rightarrow +\infty$, the ratio of probabilities becomes,

$$\frac{P(\gamma)}{P(\alpha)} \rightarrow \exp[2Jh_i(S_i^\gamma - S_i^\alpha)] \quad (36)$$

showing that the equilibrium distribution is that of the standard Ising model with twice the nearest-neighbor coupling ($J \rightarrow 2J$). Note, however, that when $K \rightarrow +\infty$ the time scale for a spin flips diverges so that if the limit is taken with the number of sweeps (and system size) held fixed then the spin configuration is fixed. Finally, when $K \rightarrow -\infty$, we have that $P(\gamma)/P(\alpha) \rightarrow 1$ showing that the model behaves as a non-interacting (infinite temperature) system.

For $0 < K < \infty$ the equilibrium distribution does not satisfy detailed balance with respect to the dynamics and one must solve the global balance equations,

$$\sum_{\gamma} [P(\gamma)A(\gamma \rightarrow \alpha) - P(\alpha)A(\alpha \rightarrow \gamma)] = 0,$$

which can be rewritten as,

$$\sum_{\gamma} \left[\frac{P(\gamma)}{P(\alpha)} A(\gamma \rightarrow \alpha) - A(\alpha \rightarrow \gamma) \right] = 0. \quad (37)$$

Let α be an arbitrary initial state, $\alpha = \{S_j^\alpha\}$ and let $\alpha(i) \equiv \gamma$ refer to the state obtained from α by flipping spin S_i . From Eq. (33), global balance takes the form,

$$\sum_i \left[\frac{P(\alpha(i))}{P(\alpha)} \frac{\exp(Jh_i^\alpha S_i^\alpha - K)}{2 \cosh(Jh_i^\alpha - K S_i^\alpha)} - \frac{\exp(-Jh_i^\alpha S_i^\alpha - K)}{2 \cosh(Jh_i^\alpha + K S_i^\alpha)} \right] = 0,$$

which can be simplified to,

$$\sum_i \left[\frac{P(\alpha(i))}{P(\alpha)} \frac{\exp(Jh_i S_i)}{\cosh(Jh_i - K S_i)} - \frac{\exp(-Jh_i S_i)}{\cosh(Jh_i + K S_i)} \right] = 0. \quad (38)$$

Superscripts are dropped in the above equation and what follows since all spins belong to configuration α .

The transition probability factors in Eq. (38) can be expanded in terms of spin couplings involving the flipped spin, S_i , and its four nearest neighbors,

$$\begin{aligned} \frac{\exp(\pm Jh_i S_i)}{\cosh(Jh_i \mp K S_i)} = \exp \left(\pm J_1 S_i \sum_{\langle j,i \rangle A} S_j - J_2 \sum_{\langle j,k,i \rangle E} S_j S_k - J_3 \sum_{\langle j,k,i \rangle F} S_j S_k \pm T_4 S_i \sum_{\langle j,k,l,i \rangle B} S_j S_k S_l \right. \\ \left. - F_4 \sum_{\langle j,k,l,m,i \rangle G} S_j S_k S_l S_m + C \right) \end{aligned} \quad (39)$$

where $\sum_{\langle \dots, i \rangle X}$ is summation among the neighbors of spin i of type X as shown in Fig. 9. To simplify the notation, spin couplings are denoted with bracketed, boldface letters as shown in Fig. 9 and written explicitly here:

$$\begin{aligned} [\mathbf{A}] &= S_i \sum_{\langle j,i \rangle A} S_j & [\mathbf{B}] &= S_i \sum_{\langle j,k,l,i \rangle B} S_j S_k S_l & [\mathbf{C}] &= S_i \sum_{\langle j,k,l,i \rangle C} S_j S_k S_l & [\mathbf{D}] &= S_i \sum_{\langle j,k,l,i \rangle D} S_j S_k S_l \\ [\mathbf{E}] &= \sum_{\langle j,k,i \rangle E} S_j S_k & [\mathbf{F}] &= \sum_{\langle j,k,i \rangle F} S_j S_k & [\mathbf{G}] &= \sum_{\langle j,k,l,m,i \rangle G} S_j S_k S_l S_m & [\mathbf{H}] &= S_i \sum_{\langle j,i \rangle H} S_j \\ [\mathbf{I}] &= S_i \sum_{\langle j,i \rangle I} S_j. \end{aligned} \quad (40)$$

Note that these couplings are implicitly functions of i .

In terms of this compact notation,

$$\frac{\exp(\pm J h_i S_i)}{\cosh(J h_i \mp K S_i)} = \exp\left(\pm J_1[\mathbf{A}] - J_2[\mathbf{E}] - J_3[\mathbf{F}] \pm T_4[\mathbf{B}] - F_4[\mathbf{G}] + C\right), \quad (41)$$

where C is a constant.

Expanding both sides of the above equation and comparing like terms yields expressions for the coupling coefficients in terms of J and K ,

$$J_1 = J + \frac{1}{8} \log \frac{\cosh(2J + K)}{\cosh(2J - K)} + \frac{1}{16} \log \frac{\cosh(4J + K)}{\cosh(4J - K)}, \quad (42)$$

$$T_4 = \frac{1}{16} \log \frac{\cosh(4J + K)}{\cosh(4J - K)} - \frac{1}{8} \log \frac{\cosh(2J + K)}{\cosh(2J - K)}, \quad (43)$$

$$J_2 = \frac{1}{8} \log[\cosh(4J + K) \cosh(4J - K)] - \frac{1}{4} \log \cosh(K), \quad (44)$$

$$J_3 = \frac{1}{16} \log[\cosh(4J + K) \cosh(4J - K)] - \frac{1}{8} \log \cosh(K), \quad (45)$$

$$F_4 = \frac{3}{8} \log \cosh(K) - \frac{1}{4} \log[\cosh(2J + K) \cosh(2J - K)] + \frac{1}{16} \log[\cosh(4J + K) \cosh(4J - K)]. \quad (46)$$

Except for J_1 these couplings are identical to the couplings appearing in the Hamiltonian for the equilibrium state of parallel dynamics, Eqs. (18)-(22). However, it is important to note that these dynamical coupling coefficients for sequential dynamics are not the same as the coupling coefficients appearing in the sequential Hamiltonian, which we now derive perturbatively in J . We begin by expanding the dynamical coupling coefficients to fourth order in J ,

$$J_1 = [\tanh(K) + 1]J + \frac{10}{3} [\tanh^3(K) - \tanh(K)]J^3 + O[J^5], \quad (47)$$

$$T_4 = [2 \tanh^3(K) - 2 \tanh(K)]J^3 + O[J^5], \quad (48)$$

$$J_2 = [2 - 2 \tanh^2(K)]J^2 + [-16 \tanh^4(K) + \frac{64 \tanh^2(K)}{3} - \frac{16}{3}]J^4 + O[J^6], \quad (49)$$

$$J_3 = \frac{J_2}{2} = [1 - \tanh^2(K)]J^2 + [-8 \tanh^4(K) + \frac{32 \tanh^2(K)}{3} - \frac{8}{3}]J^4 + O[J^6], \quad (50)$$

$$F_4 = [-6 \tanh^4(K) + 8 \tanh^2(K) - 2]J^4 + O[J^6]. \quad (51)$$

Inserting the expansion of the transition probability, Eq. (41), in the global balance equation, Eq. (38), yields,

$$\sum_i \left[\frac{P(\alpha(i))}{P(\alpha)} \exp(J_1[\mathbf{A}] - J_2[\mathbf{E}] - J_3[\mathbf{F}] + T_4[\mathbf{B}] - F_4[\mathbf{G}]) - \exp(-J_1[\mathbf{A}] - J_2[\mathbf{E}] - J_3[\mathbf{F}] - T_4[\mathbf{B}] - F_4[\mathbf{G}]) \right] = 0. \quad (52)$$

We now make the ansatz that $P(\alpha)$ can be written in Gibbsian form with a Hamiltonian potentially containing all even order spin couplings,

$$-\mathcal{H} = \tilde{J}_1 \sum_{\langle i,j \rangle 1} S_i S_j + \tilde{J}_2 \sum_{\langle i,j \rangle 2} S_j S_k + \tilde{J}_3 \sum_{\langle i,j \rangle 3} S_j S_k + \tilde{T}_4 \sum_{\langle i,j,k,l \rangle \perp} S_i S_j S_k S_l + \dots \quad (53)$$

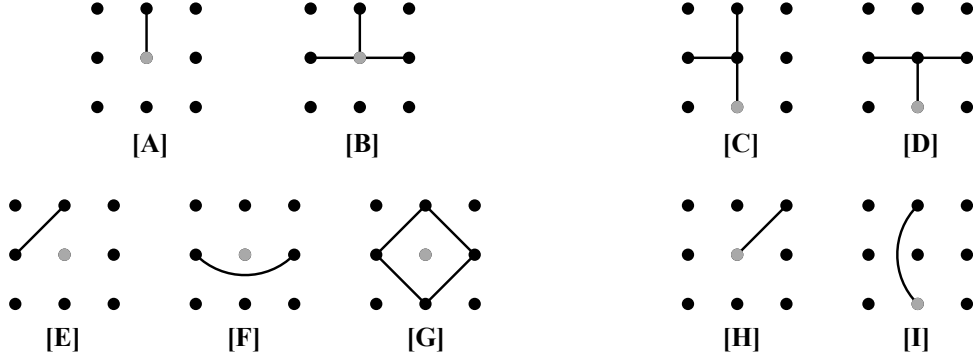


Figure 9. The dynamical interactions in the expansion of the transition probabilities are shown on the left while additional interactions appearing in the Hamiltonian are shown on the right. All interaction types are labelled with boldface letters. The grey lattice site represents the flipped spin i . All the interactions include all distinct rotations around the grey site and, in the case of [C], reflection around the vertical axis. There are 4 equivalent interactions for type [A], 4 for [B], 8 for [C], 4 for [D], 4 for [E], 2 for [F], 1 for [G], 4 for [H] and 4 for [I].

The summations in the terms that are explicitly written are defined above in Sec. IV A (see Eq. (17) and Fig. 5) and couplings in the sequential Hamiltonian are written with tildes. Given this ansatz, the ratio of probabilities is,

$$\frac{P(\alpha(i))}{P(\alpha)} = \exp \left[-2(\tilde{J}_1[\mathbf{A}] + \tilde{T}_4[\mathbf{B}] + \tilde{T}_4[\mathbf{C}] + \tilde{T}_4[\mathbf{D}] + \tilde{J}_2[\mathbf{H}] + \tilde{J}_3[\mathbf{I}]) \right]. \quad (54)$$

Inserting this expression in the global balance equation, (52), yields,

$$\sum_i \left[\exp[(-2\tilde{J}_1 + J_1)[\mathbf{A}] + (-2\tilde{T}_4 + T_4)[\mathbf{B}] - 2\tilde{T}_4[\mathbf{C}] - 2\tilde{T}_4[\mathbf{D}] - 2\tilde{J}_2[\mathbf{H}] - 2\tilde{J}_3[\mathbf{I}] - J_2[\mathbf{E}] - J_3[\mathbf{F}] - F_4[\mathbf{G}]] \right. \\ \left. - \exp(-J_1[\mathbf{A}] - T_4[\mathbf{B}] - J_2[\mathbf{E}] - J_3[\mathbf{F}] - F_4[\mathbf{G}]) \right] = 0 \quad (55)$$

We now explicitly expand all the couplings as series in the dynamic coupling, J . The coefficients of each series are represented by lower case letters and subscripts corresponding to the name of the coupling while the power in J is indicated with a superscript. Thus, for example, the nearest-neighbor coupling in the dynamical rule is,

$$J_1(J) = j_1^1 J + j_1^2 J^2 + j_1^3 J^3 + \dots \quad (56)$$

where, from Eq. (47), $j_1^1 = [\tanh(K) + 1]$, $j_1^2 = 0$, and $j_1^3 = \frac{10}{3}[\tanh^3(K) - \tanh(K)]$. The corresponding coefficients of the couplings in the Hamiltonian, $\tilde{j}_1^n, \tilde{j}_2^n, \tilde{j}_3^n, \tilde{t}_4^n$ are the quantities we wish to solve for.

Expanding Eq. (55) to first order in J yields,

$$\sum_i \left[(2\tilde{j}_1^1 - 2j_1^1)[\mathbf{A}] + 2\tilde{t}_4^1([\mathbf{B}] + [\mathbf{C}] + [\mathbf{D}]) + 2\tilde{j}_2^1[\mathbf{H}] + 2\tilde{j}_3^1[\mathbf{I}] \right] = 0 \quad (57)$$

The sums over the four distinct interaction terms, $[\mathbf{A}]$, $([\mathbf{B}] + [\mathbf{C}] + [\mathbf{D}])$, $[\mathbf{H}]$, and $[\mathbf{I}]$ must vanish independently, thus to first order in J ,

$$\tilde{j}_1^1 = j_1^1 = [\tanh(K) + 1], \quad (58)$$

while the coefficients \tilde{j}_2^1 , \tilde{j}_3^1 and \tilde{t}_4^1 are all zero. Using the solutions of order J and expanding Eq. (55) to second order in J yields,

$$\sum_i \left[2\tilde{j}_1^2[\mathbf{A}] + 2\tilde{t}_4^2([\mathbf{B}] + [\mathbf{C}] + [\mathbf{D}]) + 2\tilde{j}_2^2[\mathbf{H}] + 2\tilde{j}_3^2[\mathbf{I}] \right] = 0, \quad (59)$$

so that \tilde{j}_1^2 , \tilde{j}_2^2 , \tilde{j}_3^2 and \tilde{t}_4^2 all vanish.

Note that $2\sum_i[\mathbf{B}] = \sum_i[\mathbf{C}] = 2\sum_i[\mathbf{D}]$ because of the extra reflection symmetry of $[\mathbf{C}]$, which allows us to eliminate $[\mathbf{C}]$ and $[\mathbf{D}]$ from the equations in favor of $[\mathbf{B}]$. The relations between these terms holds due to the summation over i and marks the first appearance where global balance, rather than detailed balance, must be invoked. Using the solutions at order J and J^2 , the global balance condition at order J^3 is,

$$\sum_i \left[(2\tilde{j}_1^3 - 2j_1^3)[\mathbf{A}] + (8\tilde{t}_4^3 - 2t_4^3)[\mathbf{B}] + 2\tilde{j}_2^3[\mathbf{H}] + 2\tilde{j}_3^3[\mathbf{I}] \right] = 0. \quad (60)$$

Thus, we find $\tilde{j}_2^3 = 0$, $\tilde{j}_3^3 = 0$, and $\tilde{j}_1^3 = j_1^3$, and $\tilde{t}_4^3 = t_4^3/4$. At this order products of interactions also appear. For example, one finds terms of the form $[\mathbf{A}] \cdot [\mathbf{A}] \cdot [\mathbf{A}] = 10[\mathbf{A}] + 6[\mathbf{B}]$, however, all such terms have coefficients that vanish at this order.

Thus, to order J^3 there are only two terms in the sequential Hamiltonian,

$$-\mathcal{H} = \tilde{J}_1 \sum_{\langle i,j \rangle 1} S_i S_j + \tilde{T}_4 \sum_{\langle i,j,k,l \rangle \perp} S_i S_j S_k S_l + O[J^4], \quad (61)$$

where

$$\begin{aligned} \tilde{J}_1 &= j_1^1 J + j_1^3 J^3 + O[J^4] \\ &= [\tanh(K) + 1]J + \frac{10}{3} [\tanh^3(K) - \tanh(K)]J^3 + O[J^4] \end{aligned} \quad (62)$$

and

$$\begin{aligned} \tilde{T}_4 &= \frac{t_4^3}{4} J^3 + O[J^4] \\ &= \frac{1}{2} [\tanh^3(K) - \tanh(K)]J^3 + O[J^4]. \end{aligned} \quad (63)$$

We now consider additional couplings beyond those explicitly written in the Hamiltonian, Eq. (53). It is straightforward though tedious to show that no additional terms appear up to third order in J . Consider an additional distinct coupling term in the Hamiltonian with coupling \tilde{J}_x . The ratio of the stationary probabilities before and after flipping spin S_i , Eq. (54), will include a new set of terms, distinct from the previous terms, all rooted at site i , and all having coupling coefficients \tilde{J}_x . As before, we expand \tilde{J}_x in a power series in J , $\tilde{J}_x = \tilde{j}_x^1 J + \tilde{j}_x^2 J^2 + \tilde{j}_x^3 J^3 + \dots$, and then supplement the global balance equation (55) with the new terms. Finally, one must carry out the expansion in powers of J and see that the coefficients \tilde{j}_x^1 , \tilde{j}_x^2 and \tilde{j}_x^3 all vanish. The intuitive reason why this is the case is that there are no dynamical couplings at order J^3 to balance an added term in the Hamiltonian.

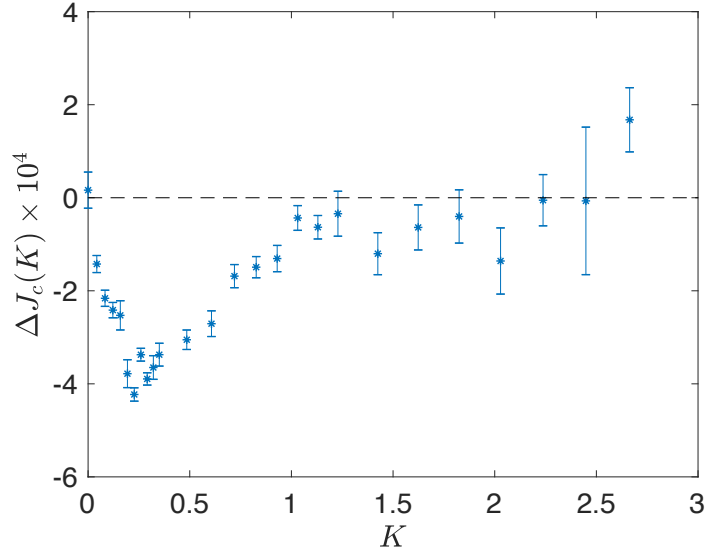


Figure 10. The difference, $\Delta J_c(K)$ between the numerical data for the critical curve for sequential dynamics and the approximation, Eq. (64), as a function of K .

On the other hand, at fourth and higher order in J , new types of interactions that are not present in the set shown in Fig. 9 appear as a result of products of couplings such as $[\mathbf{A}] \cdot [\mathbf{C}]$ and these interactions can couple spins not included in the five spin “cross”. Both long range and multi-spin couplings are expected to appear at higher order in J but as the range or number of spins increases, the leading order in J of the associated coupling constant will increase. The higher order terms in the sequential Hamiltonian are left for future research.

1. Approximation to the sequential critical curve

Here we present an approximation to the critical dynamical coupling $J_c^{(s)}(K)$ for sequential dynamics. Assume that the \tilde{T}_4 term and all higher order couplings can be neglected and that the nearest-neighbor coupling, \tilde{J}_1 is best approximated by the full expression $J_1(J, K)$ in Eq. (42) rather than the third order truncation, Eq. (62). Then our approximation for the critical curve, $J_c^{(s)}(K)$ is given by the implicit equation,

$$J_1(J_c^{(s)}(K), K) = J_c(0), \quad (64)$$

where $J_c(0) \approx 0.4407$ is the critical coupling of the ordinary Ising model. The critical curve was obtained from this equation numerically and is shown in blue (upper curve) in Fig. 1.

This approximation is surprisingly good. It is exact for both $K \rightarrow 0$ and $K \rightarrow \infty$. Figure 10 shows the difference, $\Delta J_c(K)$ between the numerical result for the critical coupling $J_c^{(s)}(K)$ and the approximation, $J_1(J_c^{(s)}(K), K) = J_c(0)$. Finite-size effects are not taken into account in the numerical results and may be responsible for some of this difference, which never exceeds 4 parts in 10^4 .

V. MEAN FIELD THEORY

In this section, the phase diagram for the kinetic Ising model with self-interaction is obtained within a mean field approximation. Mean field theory (MFT) for the equilibrium, nearest-neighbor Ising model with no self-interaction or magnetic field yields a self-consistent equation for the magnetization per spin m ,

$$m = \tanh(Jzm) \quad (65)$$

where z is the coordination number. The critical coupling J_c marking the onset of spontaneous magnetization ($|m| > 0$) occurs when $J_c z = 1$.

One can interpret the mean field equation, (65), as a dynamical equation with the magnetization on the left hand side being one time step later than the magnetization on the right hand side. Equilibrium states are obtained by setting the magnetization on the two sides of the equation equal. We can generalize the mean field dynamical equation to include self-interaction by replacing h_i in Eq. (1) by zm . The mean field dynamical equation for spin, S_i is,

$$\langle S'_i \rangle = \tanh(Jzm + KS_i), \quad (66)$$

where $\langle S'_i \rangle$ is the expected value of spin S_i at the subsequent time step. We now average over sites i to obtain the equilibrium equation for m ,

$$m = \left(\frac{1+m}{2} \right) \tanh(Jzm + K) + \left(\frac{1-m}{2} \right) \tanh(Jzm - K), \quad (67)$$

where the first and second terms on the right hand side correspond to the contributions from plus and minus spins, respectively.

Close to the critical point, an expansion in m yields an equation for the critical curve, $J_c(K)$,

$$J_c(K)z[1 + \tanh(K)] - 1 = 0. \quad (68)$$

The phase diagram obtained from Eq. (68) is plotted as the solid magenta line in Fig. 11. The value of z is adjusted so that $J_c(K=0)$ is the exact value for the two-dimensional Ising model. We see that MFT agrees qualitatively with the numerical results. Mean field theory does not distinguish between sequential and parallel dynamics so it is perhaps not surprising that the critical curve lies between the parallel and sequential critical curves. Our mean field theory captures the exact result for both dynamics that $J_c(K) \rightarrow J_c(0)/2$ as $K \rightarrow \infty$. Finally, the mean field equation (68) is the same as the mean field equation for the standard Ising model except for the factor of $[1 + \tanh(K)]$, which is precisely the first order in J correction to the nearest-neighbor coupling in the sequential Hamiltonian (see Eq. (58)).

An alternative mean field theory was obtained in [2] and is also shown in Fig. 11 as the solid green curve. These results were calculated from a mean field approximation applied to the Hamiltonian obtained

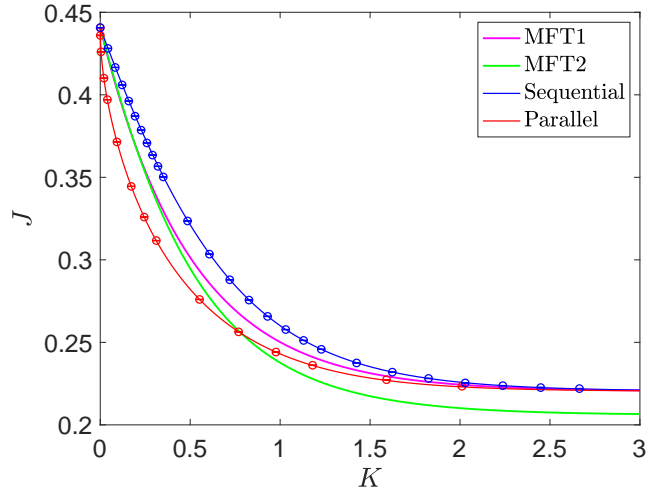


Figure 11. The phase diagram in the J - K plane showing the critical dynamical coupling obtained from mean field theories. Critical lines for parallel (red, lower) and sequential dynamics (blue, upper) are shown for comparison (see Fig. 1 for details). The magenta curve that lies between the data for sequential and parallel dynamics is the mean field theory, MFT1, obtained here (see Eq. (68)) and the green solid line that falls below the data points is mean field theory, MFT2, of Ref. [2].

for parallel dynamics (see Eq. (14)). The MFT phase plot for the parallel dynamics is adjusted so that $J_c(K=0)$ is the exact value for the two-dimensional Ising model. The qualitative behavior agrees with the other phase plots but it does not capture $J_c(K) \rightarrow J_c(0)/2$ as $K \rightarrow \infty$.

VI. DISCUSSIONS

We have studied kinetic Ising models with nearest-neighbor dynamical interaction J and self-interaction, K , and for both random sequential updating and parallel updating. These models were studied with Monte Carlo simulation and analytic methods. The equilibrium phase diagram and critical lines of both models were obtained numerically and approximated by several methods. One of these approximations is a simple mean field theory that predicts a critical line that falls between the parallel and sequential critical lines. In addition, the critical dynamics of the sequential model was studied and the prefactor of the critical divergence of the magnetization autocorrelation time was found to increase as e^{2K} . It would be interesting to investigate the addition of a self-interaction term in the dynamics of other spin models, for example the Potts and Blume-Capel models, to see how it effects the equilibrium distribution and autocorrelation times.

We have studied the Gibbs distributions describing the equilibrium states of the two models. For the parallel model, this distribution satisfies detailed balance with respect to the dynamics. The associated Hamiltonian was previously obtained [2], and involves three two-spin couplings and two four-spin couplings. The equilibrium distribution for the random sequential model does not satisfy

detailed balance with respect to the dynamics and must be obtained from the global balance equation. We developed a perturbative expansion of the sequential Hamiltonian in the dynamical coupling, J and carried it out to order J^3 . At this order the Hamiltonian features a nearest-neighbor coupling and a four-spin coupling. It is clear that at higher order, other smaller couplings, perhaps infinitely many other couplings, will appear. The nearest-neighbor coupling obtained from the perturbative expansion yields a very accurate approximation to the critical line. It would be interesting to understand the equilibrium Gibbs distribution for sequential updating more completely. Does the Hamiltonian in fact have infinitely many couplings and, if so, how do they fall off as a function of the range of interaction and the number of coupled spins?

For the parallel case we focused attention on the region near the $K = 0$ critical point, which is described by two uncoupled critical Ising models on the two sublattices of the square lattice. When the full lattice is viewed, large checkerboard regions are apparent at and near this critical point. For small, but non-vanishing K two critical lines emerge from the $K = 0$ critical point for positive and negative K , respectively. Numerical results show that these critical lines approach the $K = 0$ critical point as a power law with an exponent slightly larger than $1/2$. We proposed a finite-size scaling theory for the region near the $K = 0$ critical point that includes a new critical exponent that controls the scaling behavior in the K direction and the power-law behavior of the critical lines. We presented a heuristic argument based on the length scale for checkerboard regions as a function of K , which predicts that the exponent describing the shape of the critical lines is $1/2$. It would be interesting to understand the scaling behavior near the $K = 0$ critical point more fully. Is the finite-size scaling theory correct? If so, what is the actual scaling exponent and can it be related to known Ising critical exponents?

When self-interaction is large and positive, the equilibrium states of the sequential and parallel models both reduce to a nearest-neighbor Ising model with twice the dynamical coupling strength [18]. The equivalence of the two updating schemes can be understood intuitively from the fact that spin-flips occur exponentially rarely so that a parallel update becomes equivalent to a single sweep of sequential updates—in both cases almost no spin flips occur.

ACKNOWLEDGMENTS

We thank Karen Abbott, Shadi Esmaili, Alan Hastings, and Andrew Noble for useful discussions. The work was supported in part by NSF grant DMS-1840221.

[1] G. Grinstein, C. Jayaprakash, and Yu He. Statistical mechanics of probabilistic cellular automata. *Phys. Rev. Lett.*, 55:2527–2530, 1985.

- [2] E. N. M. Cirillo, P. Y. Louis, W. M. Ruszel, and C. Spitoni. Effect of self-interaction on the phase diagram of a Gibbs-like measure derived by a reversible probabilistic cellular automata. *Chaos, Solitons and Fractals*, 64:36 – 47, 2014.
- [3] M. Stern, H. Sompolinsky, and L. F. Abbott. Dynamics of random neural networks with bistable units. *Phys. Rev. E*, 90:062710, 2014.
- [4] S. Bornholdt. Expectation bubbles in a spin model of markets: Intermittency from frustration across scales. *International Journal of Modern Physics C*, 12:667–674, 2001.
- [5] F. Caccioli, S. Franz, and M. Marsili. Ising model with memory: coarsening and persistence properties. *Journal of Statistical Mechanics: Theory and Experiment*, 2008(07):P07006, 2008.
- [6] T. Okuyama, T. Sonobe, K. Kawarabayashi, and M. Yamaoka. Binary optimization by momentum annealing. *Phys. Rev. E*, 100:012111, 2019.
- [7] A. E. Noble, J. Machta, and A. Hastings. Emergent long-range synchronization of oscillating ecological populations without external forcing described by Ising universality. *Nature Communications*, 6(1):6664, 2015.
- [8] E. N. M. Cirillo, F. R. Nardi, and A. D. Polosa. Magnetic order in the Ising model with parallel dynamics. *Phys. Rev. E*, 64:057103, 2001.
- [9] P. Y. Louis. *Probabilistic cellular automata : stationary measures, associated Gibbs measures and ergodicity*. Theses, Université des Sciences et Technologie de Lille - Lille I, 2002.
- [10] K. Binder. Critical properties from Monte Carlo coarse graining and renormalization. *Phys. Rev. Lett.*, 47:693–696, 1981.
- [11] W. Selke. Critical Binder cumulant of two-dimensional Ising models. *The European Physical Journal B - Condensed Matter and Complex Systems*, 51(2):223–228, 2006.
- [12] G. Ossola and A. D. Sokal. Dynamic critical behavior of the Swendsen–Wang algorithm for the three-dimensional Ising model. *Nuclear Physics B*, 691:259, 2004.
- [13] X. Lei, J. Zheng, and X. Zhao. Monte Carlo simulations for two-dimensional Ising system far from equilibrium. *Chinese Science Bulletin*, 52(3):307–312, 2007.
- [14] M. P. Nightingale and H. W. J. Blöte. Dynamic exponent of the two-dimensional Ising model and Monte Carlo computation of the subdominant eigenvalue of the stochastic matrix. *Phys. Rev. Lett.*, 76:4548–4551, 1996.
- [15] F. Wang, N. Hatano, and M. Suzuki. Study on dynamical critical exponents of the Ising model using the damage spreading method. *Journal of Physics A: Mathematical and General*, 28(16):4543, 1995.
- [16] P. C. Hohenberg and B. I. Halperin. Theory of dynamic critical phenomena. *Rev. Mod. Phys.*, 49:435–479, 1977.
- [17] K. E. Bassler and B. Schmittmann. Critical dynamics of nonconserved Ising-like systems. *Phys. Rev. Lett.*, 73:3343–3346, 1994.

- [18] P. Dai Pra, B. Scoppola, and E. Scoppola. Sampling from a Gibbs measure with pair interaction by means of PCA. *Journal of Statistical Physics*, 149:722–737, 2012.
- [19] K. G. Wilson. The renormalization group: Critical phenomena and the Kondo problem. *Rev. Mod. Phys.*, 47:773–840, 1975.
- [20] H. J. Maris and L. P. Kadanoff. Teaching the renormalization group. *American Journal of Physics*, 46(6):652–657, 1978.